5664 *Chem. Mater.* **2009,** *21,* 5664–5673
DOI:10.1021/cm902861y

CHEMISTRY OF MATERIALS
Article

Generation of Mesoporosity in LTA Zeolites by Organosilane Surfactant for Rapid Molecular Transport in Catalytic Application

Kanghee Cho,[†,‡] Hae Sung Cho,[†] Louis-Charles de Ménorval,[§] and Ryong Ryoo*[,†,‡,∥]

[†]*Center for Functional Nanomaterials, Department of Chemistry, KAIST, Daejeon 305-701, Korea,* [‡]*Graduate School of Nanoscience and Technology (WCU), KAIST, Daejeon 305-701, Korea,* [§]*Laboratoire des Agrégats, Interfaces et Matériaux pour l'Energie. ICGM UMR-5253-CNRS, AIME. Université Montpellier II. 2 Place Eugène Bataillon, CC-1502, 34095 Montpellier Cédex 05, France, and* [∥]*KAIST Institute for the NanoCentury, Daejeon 305-701, Korea*

Received September 13, 2009. Revised Manuscript Received October 22, 2009

Hydrothermal crystallization of LTA zeolite was performed at a gel composition containing organosilane surfactant as a mesopore-generating agent. The zeolite was constructed of microporous crystalline zeolite frameworks that were penetrated by a three-dimensional disordered network of mesopores. Pore size analysis showed a gradual shift from 6 to 10 nm as the amount of the surfactant was increased. The detailed study indicated that the mesopores were templated by the organosilane surfactant, where the micelles were expanded by the excessive organosilane. Pore diameters could be further expanded to 24 nm by the addition of $EO_{20}PO_{70}EO_{20}$ triblock copolymers as pore-expanding agents. Xenon uptake and ^{129}Xe NMR measurements at 297 K revealed that the xenon diffusion into the highly mesoporous LTA zeolite could occur 200 times more rapidly compared with that of a solely microporous zeolite. The two zeolites showed a dramatic difference in product selectivity, catalytic activity, and lifetime, when they were compared after Ca^{2+} ion exchange as a catalyst for the conversion of methanol to dimethyl ether and hydrocarbons. These results are attributed to rapid transport into and out of the zeolitic micropores via mesopores. Fully open micropore−mesopore connectivity would make such hierarchically porous zeolites very attractive for applications in adsorption and catalysis.

Introduction

Zeolites are a family of crystalline aluminosilicate materials that are composed by regular arrangement of uniform micropores with a high specific surface area and good hydrothermal stability.[1] So far, 191 structure types of zeolite are known, with various Si/Al ratios, pore diameters (typically in the range of 0.3−1.3 nm),[2] pore shapes, and connectivity. Zeolites with strong acidity and supporting metal nanoparticles are widely used as shape-selective catalysts in petrochemical industry and organic synthesis.[3,4] Conventional zeolite crystals are normally in the size of a few micrometers, consisting of thousands of pores along a crystal axis. The sole presence of so many micropores often imposes a diffusion limitation for catalytic applications involving large molecules.[4] Quite a few works have been devoted in solving the diffusion limitation such as synthesis of nanocrystalline zeolites containing open mesopores in the intercrystalline void space,[5] synthesis of zeolites with mesopore−micropore hierarchical structures using hard templates,[6−8] or supramolecular soft templates,[9−12] and postsynthetic dealumination or desilication treatments.[13−16]

In particular, Choi et al.[9] reported that the mesopore diameters in MFI zeolite could be precisely controlled by the molecular size of organosilane surfactants, which were added as mesopore-generating agents into the zeolite synthesis composition. This synthesis strategy was also applied for LTA zeolite[9] and microporous aluminophosphate.[17]

*To whom correspondence should be addressed. E-mail: rryoo@kaist.ac.kr.

(1) Cundy, C. S.; Cox, P. A. *Chem. Rev.* **2003**, *103*, 663–701.
(2) International Zeolite Association Home Page. http://www.iza-online.org/.
(3) Corma, A. *Chem. Rev.* **1997**, *97*, 2373–2419.
(4) Corma, A. *J. Catal.* **2003**, *216*, 298–312.
(5) Tosheva, L.; Valtchev, V. P. *Chem. Mater.* **2005**, *17*, 2494–2513.
(6) Holland, B. T.; Abrams, L.; Stein, A. *J. Am. Chem. Soc.* **1999**, *121*, 4308–4309.
(7) Jacobsen, C. J.; Madsen, C.; Houzvicka, J.; Schmidt, I.; Carlsson, A. *J. Am. Chem. Soc.* **2000**, *122*, 7116–7117.
(8) Fan, W.; Snyder, M. A.; Kumar, S.; Lee, P. −S.; Yoo, W. C.; McCormick, A. V.; Penn, R. L.; Stein, A.; Tsapatsis, M. *Nat. Mater.* **2008**, *7*, 984–991.
(9) Choi, M.; Cho, H. S.; Srivastava, R.; Venkatesan, C.; Choi, D. −H.; Ryoo, R. *Nat. Mater.* **2006**, *5*, 718–723.
(10) Wang, H.; Pinnavaia, T. J. *Angew. Chem., Int. Ed.* **2006**, *45*, 7603–7606.
(11) Serrano, D. P.; Aguado, J.; Escola, J. M.; Rodriguez, J. M.; Peral, Á. *Chem. Mater.* **2006**, *18*, 2462–2464.
(12) Xiao, F. S.; Wang, L. F.; Yin, C. Y.; Lin, K. F.; Di, Y.; Li, J. X.; Xu, R. R.; Su, D. S.; Schlogl, R.; Yokoi, T.; Tatsumi, T. *Angew. Chem., Int. Ed.* **2006**, *45*, 3090–3093.
(13) Janssen, A. H.; Schmidt, I.; Jacobsen, C. J. H.; Koster, A. J.; de Jong, K. P. *Microporous Mesoporous Mater.* **2003**, *65*, 59–75.
(14) Ogura, M.; Shinomiya, S. -Y.; Tateno, J.; Nara, Y.; Kikuchi, E.; Matsukata, M. *Chem. Lett.* **2000**, *29*, 882–883.
(15) Groen, J. C.; Jansen, J. C.; Moulijin, J. A.; Pérez-Ramírez, J. *J. Phys. Chem. B* **2004**, *108*, 13062–13065.
(16) Groen, J. C.; Bach, T.; Ziese, U.; Paulaime-, A. M.; de Jong, K. P.; Moulijin, J. A.; Pérez-Ramírez, J. *J. Am. Chem. Soc.* **2005**, *127*, 10792–10793.
(17) Choi, M.; Srivastava, R.; Ryoo, R. *Chem. Commun.* **2006**, 4380–4382.

 Published on Web 11/04/2009

However, except for MFI, very little is still known about the relation between the surfactant structure and mesopore diameters. The addition of organosilane surfactant into an LTA synthesis composition led to the generation of particle morphologies exhibiting surface roughness, which looked like an aggregation of numerous tiny nanocrystals. The pore size analysis showed a somewhat broad distribution centered at 10 nm, and the 10 nm diameters were too large to explain by molecular size of the surfactant.

As reported by Choi et al., the mesoporous MFI zeolites synthesized by organosilane surfactants exhibited high catalytic activities in various acid−catalytic reactions involving bulky molecules that could not enter the zeolite micropores.[9,18] The catalytic reactions indicated that the acidity of the mesopore walls was not so strong as compared with bulk MFI frameworks.[18,19] Nevertheless, it was sufficiently strong for catalytic reactions requiring moderate acidity. The synthesis of mesoporous zeolites by Choi et al. was initially motivated for catalytic applications in large molecular reactions.[9] Srivastava et al.[20] later discovered that the mesoporous MFI zeolite could maintain a much longer catalytic lifetime in several cases of small molecular reactions that occurred certainly inside zeolitic micropores. The increased catalytic lifetime was ascribed to rapid removal of reaction intermediates out of zeolite micropores before polymerization to the catalyst deactivating cokes.[20,21] A similar effect of mesopores was reported by Bjørgen et al.[22] in the catalytic conversion of methanol to hydrocarbons over an MFI zeolite, which was desilicated for mesopore generation. Besides, it was reported that catalytic activities and selectivity were changed because of mesopores in hierarchical MFI zeolites.[22] However, most works in the literature assigned the improved catalytic performance of mesoporous zeolites to improved molecular transport without evidence of transport properties. A recent review by Perez-Ramirez et al. stressed the lack of diffusion studies in research associated with mesoporous zeolites.[23]

Because of the significance of the mesopores in catalytic applications of zeolites, several laboratories have investigated the effects of mesopore generation on molecular diffusion in MFI zeolites possessing mesopores. Christensen et al.[24] reported that a hierarchical MFI zeolite, which was synthesized in a nanocarbon template, adsorbed isobutene gas significantly faster than conventional MFI zeolite. Groen et al.[25] measured the rate of neopentane uptake by a desilicated MFI zeolite and reported that the adsorption rate was increased to about 100 times compared to that of a conventional MFI zeolite (i.e., solely microporous). Liu et al.[26] used hyperpolarized ^{129}Xe NMR spectroscopy to investigate xenon exchange between mesopores and micropores in a starch-templated MFI zeolite. They reported that xenon exchange between the two kinds of pore systems occurred rapidly in the NMR time scale, using a variable-temperature NMR experiment and two-dimensional (2-D) exchange spectroscopy.

The present work was undertaken to investigate how mesopores are generated in LTA zeolites by organosilane surfactants. A specific issue was if the mesopores were really "templated" by the surfactant micelles or because of the formation of intercrystalline void space when presynthesized zeolite nanocrystals were packed. Another important issue was whether mesoporous zeolite materials synthesized in this way could have fully open connectivity between mesopores and micropores. To answer these questions, we performed an extensive study for the control of mesoporosity in hierarchical LTA zeolites by varying the amount of organosilane surfactant. The mesopore shape and connectivity was visualized by a TEM imaging technique after Pt nanowires were generated along the mesoporous channels. The mechanism of the surfactant to generate mesopores was investigated by analyzing a series of nitrogen adsorption isotherms, which were taken from the samples as synthesized, washed with methanol, and calcined in air. Possibilities for controlling mesopore diameters beyond 10 nm were also investigated using $EO_{20}PO_{70}EO_{20}$ triblock copolymers as a pore expanding agent. Furthermore, diffusion of xenon was investigated with ^{129}Xe NMR spectroscopy for a series of LTA zeolite samples having various degrees of mesoporosity.

The choice of ^{129}Xe NMR is particularly suited for a diffusion study in LTA zeolite. The zeolite structure is composed of α-cages, which are 1.1 nm in diameter and accessible through eight-membered ring apertures (0.42 nm in diameter, Figure 1).[27] The α-cage aperture is slightly smaller than the size of xenon atom (0.44 nm in diameter). According to earlier studies using ^{129}Xe NMR spectroscopy,[28−33] xenon adsorption into conventional LTA zeolites through the small pore apertures required

(18) Shetti, V. N.; Kim, J.; Srivastava, R.; Choi, M.; Ryoo, R. *J. Catal.* **2008**, *254*, 296–303.
(19) Suzuki, K.; Aoyagi, Y.; Katada, N.; Choi, M.; Ryoo, R.; Niwa, M. *Catal. Today* **2008**, *132*, 38–45.
(20) Srivastava, R.; Choi, M.; Ryoo, R. *Chem. Commun.* **2006**, 4489–4491.
(21) Choi, M.; Na, K.; Kim, J.; Sakamoto, Y.; Terasaki, O.; Ryoo, R. *Nature* **2009**, *461*, 246–250.
(22) Bjørgen, M.; Joensen, F.; Holm, M. S.; Olsbye, U.; Lillerud, K. −P.; Svelle, S. *Appl. Catal. A* **2008**, *345*, 43–50.
(23) Pérez-Ramírez, J.; Christensen, C. H.; Egeblad, K.; Christensen, C. H.; Groen, J. C. *Chem. Soc. Rev.* **2008**, *37*, 2530–2542.
(24) Christensen, C. H.; Johannsen, Kim; Törnqvist, E.; Schmidt, I.; Topsøe, H.; Christensen, C. H. *Catal. Today* **2007**, *128*, 117–122.
(25) Groen, J. C.; Zhu, W.; Brouwer, S.; Huynink, S. J.; Kapteijn, F.; Moulijn, J. A.; Pérez-Ramírez, J. *J. Am. Chem. Soc.* **2007**, *129*, 355–360.
(26) Liu, Y.; Zhang, W.; Liu, Z.; Xu, S.; Wang, Y.; Xie, Z.; Han, X.; Bao, X. *J. Phys. Chem. C* **2008**, *112*, 15375–15381.
(27) Breck, D. W. *Zeolite Molecular Sieves*; Wiley and Sons: New York, 1974.
(28) Samant, M. G.; de Ménorval, L. C.; Dalla, R. A.; Boudart, M. *J. Phys. Chem.* **1988**, *92*, 3937–3938.
(29) Chmelka, B. F.; Raftery, D.; McCormick, A. V.; de Ménorval, L. C.; Levine, R. D.; Pines, A. *Phys. Rev. Lett.* **1991**, *66*, 580–583.
(30) Jameson, C. J.; Jameson, A. K.; Gerald, R.; de Dios, A. C. *J. Chem. Phys.* **1992**, *96*, 1676–1689.
(31) Ryoo, R.; de Ménorval, L. C.; Kwak, J. H.; Figueras, F. *J. Phys. Chem.* **1993**, *97*, 4124–4127.
(32) Larsen, R. G.; Shore, J.; Schmidt-Rohr, K.; Emsley, L.; Long, H.; Pines, A.; Janicke, M.; Chmelka, B. F. *Chem. Phys. Lett.* **1993**, *214*, 220–226.
(33) Jameson, A. K.; Jameson, C. J.; Gerald, R. E. *J. Chem. Phys.* **1994**, *101*, 1775–1786.

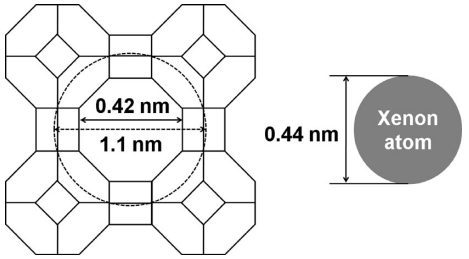

Figure 1. Schematic representation of LTA zeolite structure, comparing the diameters of the α-cage (dashed line), aperture, and xenon atom.

many days of xenon contact until reaching equilibrium at room temperature. The xenon exchange between adjacent α-cages was slow in the ^{129}Xe NMR time scale, so that the pore environment could be probed by the chemical shift before migration into adjacent cages. The ^{129}Xe NMR chemical shift progressively increased because of the xenon−xenon interaction as the number of xenon atoms occluded in the same cage increased. Thus, xenon atoms adsorbed in α-cages exhibited several separated ^{129}Xe NMR lines with different chemical shifts, depending on the number of xenon atoms present in the same α-cage. Because of this, it was expected that the diffusion of xenon atoms into α-cages would properly be monitored by the intensity of the ^{129}Xe NMR signals. The ^{129}Xe NMR signals were obtained from the series of hierarchically porous LTA zeolite samples. The ^{129}Xe NMR peaks were used as a means of visualizing the amount of xenon atoms entering zeolite α-cages during a certain period of time. The ^{129}Xe NMR result was correlated to the rate of xenon uptake by the zeolite. Increase in the diffusion rate due to mesoporosity was discussed to explain changes in the catalytic selectivity in the conversion of methanol to dimethyl ether (DME) and light olefins. This reaction has been chosen in combination with ^{129}Xe NMR for the diffusion study in LTA zeolite because DME and xenon have very similar kinetic diameters. The Lennard−Jones σ parameters for DME and xenon are 0.43 and 0.44 nm, respectively.[34]

Experimental Section

Synthesis of LTA Zeolites. 3-(Trimethoxysilyl)propylhexadecyldimethylammonium chloride (TPHAC) was used as an organosilane surfactant for the generation of mesoporosity in LTA zeolite. The TPHAC was obtained as a 56 wt % solution in methanol, following the synthesis procedure described elsewhere.[35] Four samples of LTA zeolite were hydrothermally synthesized at the gel compositions of 100 SiO_2/333 Na_2O/67.0 Al_2O_3/20000 H_2O/*n* TPHAC, where *n* was varied from 0 to 2, 4, and 8. The zeolite samples thus synthesized were denoted as NaA-0, NaA-2, NaA-4, and NaA-8, respectively. Here, "Na" means the cationic form of LTA zeolite, and the numbers following "NaA" refer to the TPHAC mole numbers. The hydrothermal synthesis procedure for NaA-*n* can be briefed as follows: a homogeneous solution was prepared by dissolving $n \times 0.235$ g of 56 wt % TPHAC solution, 7.90 g of sodium metasilicate nonahydrate (≥98%, Sigma-Aldrich), and 3.23 g of sodium hydroxide in 66.7 g of distilled water. Another solution was prepared by dissolving 3.56 g of sodium aluminate (Na_2O 53.0 wt %, Al_2O_3 42.5 wt %, Riedel-de Haën) into 33.3 g of distilled water. The two solutions were mixed at once with vigorous shaking. After shaking for 5 min, the resultant gel was heated for 4 h at 373 K with magnetic stirring. Products were filtered, washed with distilled water, dried in an oven at 373 K, and calcined at 823 K for 3 h.

Ca^{2+} ion exchange of NaA-*n* was performed as follows: 1 g of NaA-*n* was dispersed in 200 mL 1 M $Ca(NO_3)_2 \cdot 4H_2O$ solution for 3 h, with magnetic stirring at 333 K. This treatment was repeated three times in all, collecting sample by filtration each time. The ion-exchanged zeolite was dried in an oven at 373 K. The samples are designated as CaA-*n*.

A pore expansion experiment was carried out with poly(alkylene oxide)-based triblock copolymer Pluronic P123 ($EO_{20}PO_{70}EO_{20}$, MW = 5800, BASF) as a pore expanding agent. The synthesis procedure is the same as for NaA-*n*, except for the addition of P123. The gel composition was 100 SiO_2/333 Na_2O/67.0 Al_2O_3/20000 H_2O/4 TPHAC/*m* P123, where $0 \le m \le 0.8$.

XRD, SEM, and TEM. Powder X-ray diffraction (XRD) patterns were recorded by a Rigaku Multiflex diffractometer using a monochromatized X-ray beam from nickel-filtered Cu Kα radiation (40 kV, 30 mA). XRD scanning was performed under ambient conditions at steps of 0.02° and an accumulation time of 0.5 s per step.

Field emission scanning electron microscopy (SEM) images were obtained using a Hitachi S-4800 instrument. Zeolite samples were dispersed on carbon tapes, and images were taken without metal coating. For transmission electron microscopy (TEM), samples were suspended in acetone (99.5 vol %) by sonication. The suspended solutions were dropped and dried on a carbon microgrid. TEM imaging was performed at room temperature using a 300 kV electron microscope (Philips F30 Tecnai).

Mesopore Imaging by Pt TEM. Platinum nanowires were generated within the mesoporous channels after impregnation of $[Pt(NH_3)_4](NO_3)_2$. TEM images of the resultant Pt nanowires were obtained as embedded inside zeolite samples, in the same way as reported previously.[36] However, details of the Pt loading procedure had to be reoptimized for the selective generation inside mesopores (not in micropores or at the external surface). In particular, the zeolite had to be ion exchanged with Ca^{2+} prior to the impregnation of $[Pt(NH_3)_4](NO_3)_2$. When $[Pt(NH_3)_4](NO_3)_2$ was impregnated into the Na^+-form of zeolite without Ca^{2+} ion exchange, Pt nanoparticles about 2−3 nm in diameter were generated after Pt reduction with H_2 gas. The Ca^{2+} ion exchange seemed to prevent the ion exchange of $Pt(NH_3)_4^{2+}$ into the zeolite.

Nitrogen Adsorption and Pore Size Analysis. Nitrogen isotherms were measured at 77 K using a volumetric gas sorption analyzer (Quantachrome AS-1MP). Before the adsorption measurements, calcined products were outgassed for 6 h at 573 K under 10^{-4} Pa. As-synthesized and methanol washed NaA-8 samples were outgassed for 6 h at 343 K under 10^{-4} Pa. The Brunauer−Emmett−Teller (BET) equation was used to calculate the surface area from adsorption edges obtained at P/P_0 between 0.05 and 0.30. The mesopore size distributions were obtained from analyzing the adsorption branch in the N_2

(34) Hirschfelder, J. O.; Curtiss, C. F.; Bird, R. B. *Molecular Theory of Gases and Liquids*; John Wiley & Sons: New York, 1964.
(35) Hüttinger, K. J.; Jung, M. F. *Chem. Ing. Tech.* **1989**, *61*, 258–259.
(36) Ryoo, R.; Cho, S. J.; Pak, C.; Lee, J. Y. *Catal. Lett.* **1993**, *20*, 107–115.

adsorption isotherms using the Barrett−Joyner−Halenda (BJH) algorithm. The mesopore volume was calculated by subtraction from the total pore volume derived by the amount of N_2 adsorbed at $P/P_0 = 0.97$ to the micropore volume calculated by a Saito−Foley analysis.

Volumetric Adsorption of Xenon. The rate of xenon uptake by zeolite was measured with a laboratory-built volumetric apparatus (Pyrex rig) equipped with an absolute capacitance manometer (MKS Baratron Type 627B). Before measurement, 0.5 g of calcined sample was degassed under vacuum for 5 h at 723 K. After cooling to 297 K under vacuum, the sample was dosed with a known amount of xenon gas that would reach a final pressure of about 1.01×10^5 Pa. The amount of uptake was accurately measured at various times, from decreases of the xenon pressure. A large volume of xenon gas was used, so that the total pressure decrease due to uptakes should be no more than 5% of the initial pressure.

NMR Spectroscopy. ^{129}Xe NMR spectra was taken at 297 K with 0.5 g of sample, which was sealed with xenon in Pyrex tubing, after being putting in contact with 1.01×10^5 Pa xenon for 12 h at 297 K. Sample sealing was performed to allow as small a dead volume as possible, compared with the amount of zeolite sample. This was necessary to minimize the amount of xenon uptake that could take place over 1 d during ^{129}Xe NMR measurements. All ^{129}Xe NMR measurements were performed in the same way as reported elsewhere.[31] Each spectrum was recorded after signal averaging over 200000 scans at 297 K with a Bruker AMX-500 FT-NMR spectrometer (operating at 138.3 MHz for ^{129}Xe). $\pi/4$ pulses were used. The relaxation delay between pulses was given as 0.5 s. Sample spinning and field locking were not used. The chemical shift was referenced to xenon gas extrapolated to zero pressure.

Catalytic Reactions. Catalytic conversion of methanol was performed in a fixed bed Pyrex reactor at 673 K, over 0.1 g of Ca^{2+} ion-exchanged LTA zeolite. Before reaction, the catalyst was activated at 823 K for 2 h in flowing air (50 mL min^{-1}). Methanol (99.6%, Dongyang) was introduced as a saturated vapor in high-purity N_2 flow (50 mL min^{-1}) at 298 K, using a bubbling saturator. The weight hourly space velocity (WHSV) of methanol was 7.5 g g^{-1} h^{-1}. The reaction mixture was analyzed with an online gas chromatograph (GC, Younglin, Acme-6000) equipped with a flame ionization detector. The GC inlet was maintained at 373 K to avoid condensation of methanol and reaction products. A HP-Plot-Q column (J&W) was used to analyze products from methanol conversion.

Results and Discussion

Generation of Mesopores by Organosilane Surfactants. Note that NaA-0 is an LTA zeolite sample, which was synthesized by following a conventional synthesis procedure. This sample is hereafter referred to as "conventional" LTA zeolite. The other NaA-*n* samples were synthesized by following the same hydrothermal synthesis procedure, except for the addition of *n* moles of TPHAC in the synthesis composition. High-purity LTA zeolite was obtained under the synthesis condition up to the addition of 8 moles of TPHAC into the synthesis composition. Zeolite crystallization required longer times with increasing TPHAC moles. With TPHAC of more than 8 moles, the products were contaminated with an amorphous phase. As shown in Figure 2, all synthesized NaA-*n* samples for $n \leq 8$ can be characterized by the

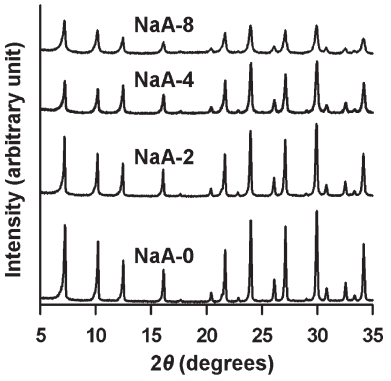

Figure 2. Powder X-ray diffraction patterns of LTA zeolites (NaA-*n*), synthesized with different amount of 3-(trimethoxysilyl)propylhexadecyldimethylammonium chloride (TPHAC) as the mesopore-generating agent. "*n*" denotes the number of TPHAC moles in the synthesis gel composition: 100 SiO_2/333 Na_2O/67.0 Al_2O_3/20000 H_2O/n TPHAC.

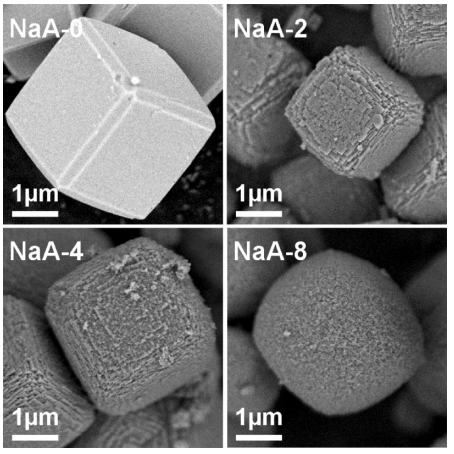

Figure 3. SEM images of NaA-*n* zeolites, showing that the morphology of hierarchical LTA zeolite is strongly affected by varying the amount of the organosilane surfactant, TPHAC.

XRD pattern of well-crystalline LTA zeolite. The only difference indicated by XRD is a gradual increase in the diffraction peak widths as the TPHAC quantity increased. This difference indicates that the size of the crystalline domain decreased because of the TPHAC addition. The decrease in crystal sizes can be confirmed by electron microscopic investigations.

As Figure 3 shows, the conventional LTA zeolite sample exhibits typical single-crystal morphologies. The crystals are in cubic shapes with truncated edges. The crystal size ranges typically from 1 to 2 μm. However, the zeolite samples synthesized by the addition of TPHAC (hereafter "TPHAC-zeolite" for brevity) show particle morphologies that are composed by numerous domains of interconnected nanocrystals. While the diameter of overall particle did not change considerably, the high-resolution SEM images show a progressive decrease in the thickness of individual nanocrystals as the amount of TPHAC was increased in the synthesis composition. In addition, the particle outline became progressively more rounded. Thus, the amount of TPHAC was a decisive factor determining the thickness of the nanocrystals. It is also remarkable that outlines of the particle shape were

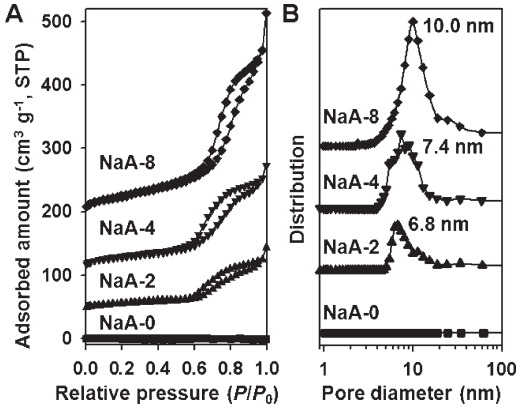

Figure 4. (a) N_2 adsorption−desorption isotherms for NaA-*n* zeolites at 77 K. Isotherms for NaA-2, 4, and 8 were vertically offset by 40, 100, and 180 $cm^3\ g^{-1}$, respectively. (b) BJH mesopore size distributions corresponding to the adsorption branch.

Table 1. Pore Textural Properties of LTA Zeolites Synthesized with Various Amounts of Organosilane Surfactants

samples[a]	S_{BET}[b] ($m^2\ g^{-1}$)	V_{meso}[c] ($cm^3\ g^{-1}$)	d_{meso}[d] (nm)
NaA-0	N.D.[e]	N.D.[e]	N.D.[e]
NaA-2	52	0.13	6.8
NaA-4	96	0.24	7.4
NaA-8	155	0.42	10.0

[a] Samples are designated by NaA-*n*, where *n* is the mole number of organosilane surfactant TPHAC in the synthesis gel composition: 100 SiO_2/333 Na_2O/67.0 Al_2O_3/20000 H_2O/*n* TPHAC. [b] S_{BET} is the BET surface area obtained from N_2 adsorption isotherm in the relative pressure range of 0.05−0.20. S_{BET} is almost same as the surface area of mesopores because the micropores of LTA zeolite are not accessible for N_2 molecules. [c] Mesopore volume corresponding to pore diameters in the range of 1.7−50.0 nm. [d] Mesopore diameter calculated from the adsorption branch using the BJH method. [e] Not determined. Data are not given explicitly.

still similar to the truncated cubes, up to 4 TPHAC. As judged from the apparently crystal-like outlines, the zeolite nanocrystals constituting a crystal-shape particle seemed to be oriented in very similar directions.

In Figure 4, the N_2 adsorption isotherm for NaA-0 shows little adsorption that can be attributed to either mesoporosity or microporosity. This is a well-known characteristic of conventional NaA zeolite. Conventional zeolite particles contain little volume of mesopores. Besides, micropore apertures in NaA zeolite are too narrow for N_2 molecules to diffuse rapidly in the equilibrium time scale of the adsorption analyzer at 77 K because of the location of Na^+ ions near the pore apertures.[27] In contrast, the TPHAC-zeolites show a steep increase in the adsorption quantity in the range of $P/P_0 = 0.6-0.9$, which is attributed to the capillary condensation of N_2 gas in mesopores. The samples show a progressive increase in mesoporosity and also BET surface area as the amount of TPHAC increases (Figure 4 and Table 1). The mesopore volume and BET area for NaA-8 were increased to 0.42 $cm^3\ g^{-1}$ and 155 $m^2\ g^{-1}$, respectively. The pore size analysis by the Barret−Joyner−Halenda (BJH) algorithm for NaA-2, 4, and 8 gave a sharp distribution of mesopores centered at 6.8, 7.4, and 10.0 nm, respectively. Therefore, these samples may be referred to as "mesoporous zeolite".

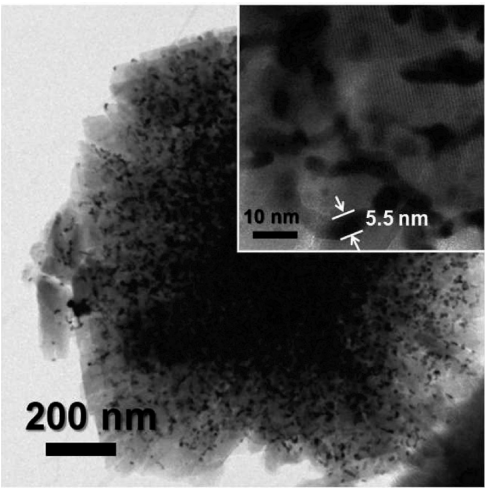

Figure 5. TEM images of NaA-2, showing Pt nanowires generated in the mesoporous channels.

All NaA-*n* zeolite samples for $n \leq 8$ were highly crystalline. No significant portion of amorphous domains was detected by TEM coupled with electron diffraction. Therefore, the mesoporosity indicated by N_2 adsorption could undoubtedly be assigned to void spaces that were located inside the micrometer-sized particle. The mesopores could be clearly visualized by the TEM imaging technique of Pt agglomerates that were generated inside the mesopores. Care was taken not to destroy the zeolite framework during the formation of Pt nanowires, which might lead to create false mesoporosity in the TEM image. Problems related to such false images were reported with Au[37] but not with Pt so far in our laboratory.[36,38] As shown in Figure 5, the Pt agglomeration was formed in the form of nanowires (dark worm-like objects) as embedded inside the micrometer-sized zeolite particles exhibiting the crystalline lattice fringes. The diameters of the Pt nanowires in NaA-2 show significant fluctuations from the mean value (approximately 5−7 nm, which is in good agreement with the pore size distribution determined by N_2 adsorption). The Pt image shows that the mesoporous channels were interconnected in a disordered, three-dimensional way. Previously, the Pt TEM imaging technique was applied for the determination of mesopore connectivity, diameters, and shapes in various materials that were composed by noncrystalline porewalls.[38] The present result in Figure 5 demonstrates that the imaging technique can be successfully extended to zeolites having hierarchically microporous−mesoporous structures, provided that experimental conditions are optimized for selective generation of Pt agglomerates in a desired pore system.

Notably, the mesopore diameters (6.8, 7.4, and 10.0 nm, obtained from N_2 adsorption) are much larger than 4 nm which can be expected from the diameter of the surfactant micelle. The discrepancy raised the following question as to the role of TPHAC for the mesopore

(37) Bore, M. T.; Pham, H. N.; Switzer, E. E.; Ward, T. L.; Fukuoka, A.; Datye, A. K. *J. Phys. Chem. B* **2005**, *109*, 2873–2880.
(38) Ko, C. H.; Ryoo, R. *Chem. Commun.* **1996**, 2467–2468.

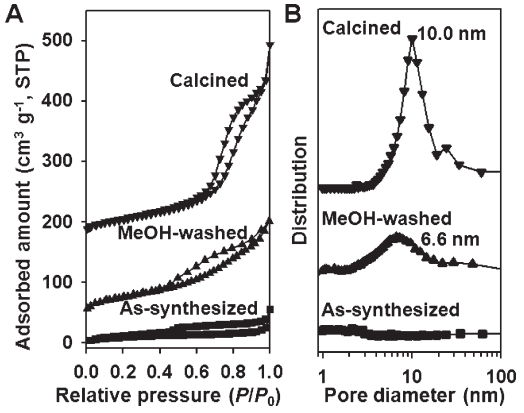

Figure 6. (a) N_2 adsorption−desorption isotherms at 77 K for as-synthesized, methanol-washed, and calcined NaA-8 zeolite. The isotherms for the methanol-washed and calcined samples were vertically offset by 50 and 150 cm^3 g^{-1}, respectively. (b) BJH mesopore size distributions corresponding to the adsorption branch.

generation: Does the organosilane surfactant work truly as a soft template for the mesopore generation as in the synthesis of the MCM-41-type mesoporous silica? If not, does the organosilane surfactant layer simply disperse the zeolite synthesis gel into tiny droplets, so that crystal growth can occur within a confined nanospace? In the former case, the mesopore diameter would be explainable with the TPHAC molecular size. In the latter case, the mesopores are generated at the intercrystalline void space. With the assumption of their random packing, the diameters of the zeolite nanocrystals would then decrease against the amount of TPHAC used in the synthesis composition, and consequently, the mesopore diameter would decrease. However, on the contrary to this assumption, the experimental result in Figure 4B shows the opposite trend.

To elucidate the mesopore-generating mechanism, NaA-8 has been selected as a target sample because it is the sample showing the steepest capillary condensation in mesopores in Figure 4A. Despite the large mesoporosity of the calcined sample, the as-synthesized sample exhibited almost no adsorption capacity for N_2 at 77 K. The adsorption capacity increased notably after the sample was thoroughly washed with methanol (Figure 6). The total pore volume was obtained as 0.22 cm^3 g^{-1} from the N_2 adsorption isotherm. The corresponding pore size analysis revealed a fairly narrow distribution centered at 6.6 nm. The pore volume and mesopore diameter are comparable to those for the calcined sample (0.42 cm^3 g^{-1}, 10.0 nm). The pore−diameter difference (3.4 nm) is very similar to the diameter of TPHAC micelle or bilayer.[9] Therefore, such a difference may be attributed to the TPHAC moiety that can remain on the mesopore walls through covalent bonding to the zeolite framework surface. Moreover, the solvent-extracted portion has been confirmed as TPHAC by ^1H NMR. On the basis of this result, it is proposed that the large mesopore diameter of hierarchical LTA zeolite should be due to its own pore-expanding effect by the organosilane surfactant as depicted in Figure 7. The excess TPHAC organosilanes may form oligomers through condensation of

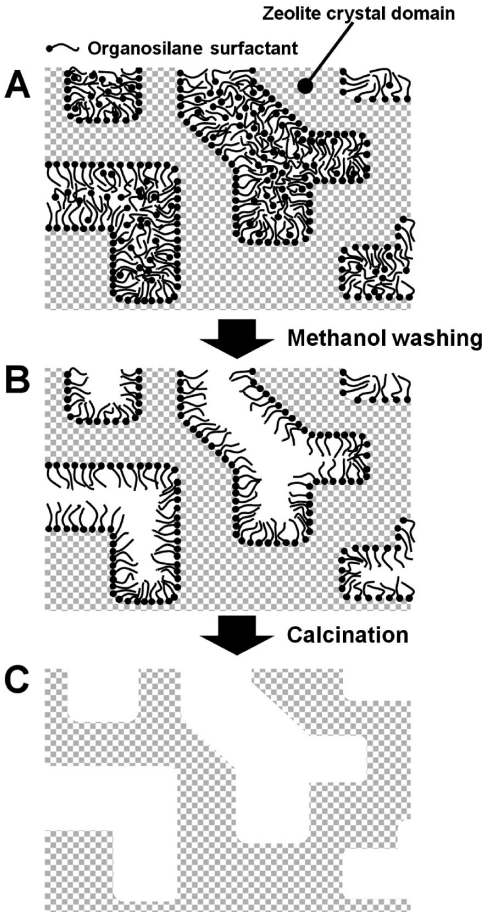

Figure 7. Schematic representation of mesopore generation in hierarchical LTA zeolite: (a) as-synthesized, (b) methanol-washed, and (c) calcined zeolite samples.

$(CH_3O)_3$ moieties. In this case, the resultant oligomers may also expand the LTA mesopores.

EO−PO−EO Triblock Copolymers as a Mesopore-Expanding Agent. The mesopore diameter can be further expanded by the addition of $EO_{20}PO_{70}EO_{20}$ triblock copolymers (BASF, Pluronic P123). As shown in Figure 8 and Table 2, the mesopore diameter increased from 7.4 to 23.7 nm according to the amount of P123. The pore volume increased from 0.24 to 0.66 cm^3 g^{-1}. This result supports that the nonionic polymers could permeate into the hydrophobic region of the TPHAC organosilane surfactant micelle, leading to expand mesopores of the zeolite. The role of P123 was similar to the pore expansion effect by trialkylamine and 1,3,5-trimethylbenzene, which are often used to expand MCM-41 and SBA-15 mesopores.[39,40]

Rapid Molecular Diffusion in Mesoporous LTA Zeolites Probed by ^{129}Xe NMR and Xenon Uptake Measurements. Figure 9A shows ^{129}Xe NMR spectra for NaA-0 and NaA-8, which were obtained after xenon contact for 12 h under 1.01×10^5 Pa at 297 K. In the case of the mesoporous NaA-8 sample, the spectrum shows a broad

(39) Sayari, A.; Yang, Y.; Kruk, M.; Jaroniec, M. *J. Phys. Chem. B* **1999**, *103*, 3651–3658.
(40) Schmidt-Winkel, P.; Lukens, W. W., Jr.; Zhao, D.; Yang, P.; Chmelka, B. F.; Stucky, G. D. *J. Am. Chem. Soc.* **1999**, *121*, 254–255.

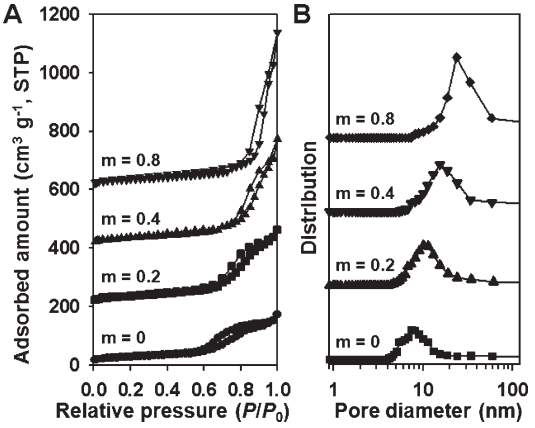

Figure 8. (a) N_2 adsorption−desorption isotherms at 77 K for hierarchical LTA zeolites synthesized with TPHAC and various amounts of P123 triblock copolymer. Each sample was synthesized at the gel compositions of 100 SiO_2/333 Na_2O/67.0 Al_2O_3/20000 H_2O/4 TPHAC/*m* P123 (*m* = 0, 0.2, 0.4, and 0.8). Adsorption isotherms for the samples synthesized with P123 (*m* = 0.2, 0.4, and 0.8) were vertically offset by 200, 400, and 600 cm^3 g^{-1}, respectively. (b) BJH mesopore size distributions corresponding to the adsorption branch.

Table 2. Pore Textural Properties of Mesoporous LTA Zeolites Synthesized with Various Amounts of P123 Triblock Copolymers

P123/TPHAC[a]	S_{BET}[b] (m^2 g^{-1})	V_{meso}[c] (cm^3 g^{-1})	d_{meso}[d] (nm)
0	96	0.24	7.4
0.05	125	0.37	10.0
0.10	127	0.47	15.3
0.20	127	0.66	23.7

[a] Each sample was prepared at the molar ratio of 100 SiO_2/333 Na_2O/67 Al_2O_3/20000 H_2O/4 TPHAC/*m* P123 ($0 < m < 0.8$). [b] S_{BET} is the BET surface area obtained from N_2 adsorption isotherm in the relative pressure range of 0.05−0.20. S_{BET} is almost same as the surface area of mesopores because the micropores of LTA zeolite are not accessible for N_2 molecules. [c] Mesopore volume corresponding to the pore diameters in the range of 1.7−50.0 nm. [d] Mesopore diameter calculated from the adsorption branch using the BJH method.

peak extended over the chemical shift range of 10−45 ppm and six narrow peaks in the range of 70−200 ppm. The broad peak can be assigned to xenon gas exchanging between the adsorption sites in the mesopores and the gas phase in the dead volume of the sample tube, similar to other materials with open pores.[41] The six peaks in 70−200 ppm are coming from xenon atoms that are located inside α-cages of the zeolite.[28−33] The first peak at 75 ppm can be assigned to the adsorption of a single xenon atom in a cage. The next peak at 95 ppm is due to the simultaneous adsorption of two xenon atoms in a same cage. The latter is increased by 20 ppm in chemical shift due to xenon−xenon interaction in the same cage. Similarly, the other peaks appearing at 115, 135, 160, and 190 ppm can be assigned to the adsorption of 3, 4, 5, and 6 xenon atoms in same cages, respectively. These peaks are well resolved because the exchange of xenon between α-cages is very slow during the NMR time scale. In the case of the conventional NaA-0 zeolite, the broad peak at 34 ppm is not detected because of the absence of mesopores. Instead, there is a very sharp signal near 0 ppm, which comes from

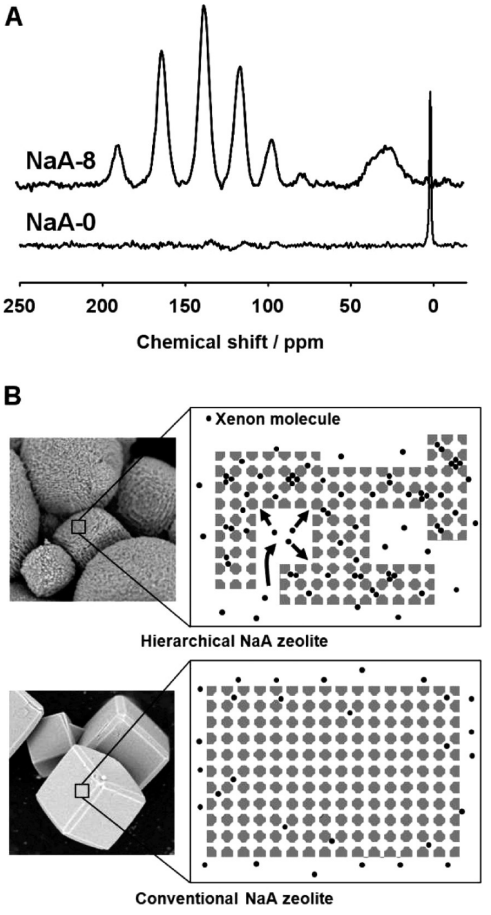

Figure 9. (a) ^{129}Xe NMR spectra of hierarchical LTA zeolite (NaA-8) and conventional LTA zeolite (NaA-0). Each spectrum was accumulated for 1 d, after xenon contact for 12 h under 1.01×10^5 Pa at 297 K. (b) Schematic illustration of xenon diffusion in hierarchical and conventional LTA zeolite crystals. Small dots indicate xenon atoms.

xenon gas in the dead volume of the sample cell. Note that the NMR signals in 70−200 ppm are almost undetectably low in intensity. This result indicates that xenon diffusion into α-cages is very slow. The slow diffusion into the conventional NaA zeolite is in good agreement with previous ^{129}Xe NMR reports on bulk NaA zeolite. Xenon can be adsorbed reversibly on bulk NaA zeolite at 673 K. Upon cooling to room temperature, we find the adsorbed xenon atoms are retained as occluded in α-cages.

The ^{129}Xe NMR spectra in Figure 9A indicate a remarkable difference in the xenon adsorption rate between NaA-0 and NaA-8 zeolites. The hierarchically porous NaA-8 zeolite exhibited a relatively much faster xenon adsorption than the conventional zeolite counterpart. On the basis of this result, it is reasonable that the generation of mesopores in NaA-8 led to a marked decrease in the crystal thickness, resulting in a marked decrease in the required diffusion path lengths (Figure 9B). In other words, the hierarchical LTA zeolite had significantly extended crystal surfaces through which xenon could diffuse into thin crystals. The α-cages at the mesopore walls must be fully accessible for xenon adsorption. That is, the xenon adsorption occurred very easily because of the micropore−mesopore connectivity in the hierarchically porous zeolites.

(41) Pietrass, T.; Kneller, J. M.; Assink, R. A.; Anderson, M. T. *J. Phys. Chem. B* **1999**, *103*, 8837–8841.

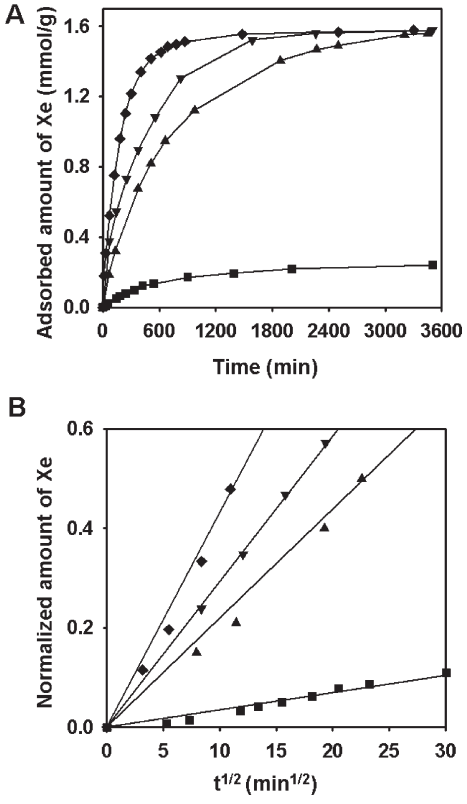

Figure 10. (a) Xenon uptake curves: NaA-0(■), NaA-2(▲), NaA-4(▼), and NaA-8(♦) in 1.01×10^5 Pa xenon at 298 K. Solid lines are guide lines for eyes. (b) Normalized amount of adsorption profiles in a short time domain. Straight lines were derived from fitting by eq 2.

For a quantitative analysis of the diffusion rates, the amount of xenon uptake was measured as a function of time under the constant pressure of 1.01×10^5 Pa at 298 K. As the result in Figure 10 shows, the xenon uptake by the mesoporous NaA-8 sample reached more than 95% of the equilibrium capacity within 12 h. As the mesoporosity was decreased as in NaA-4 and NaA-2, the longer equilibration times were required. The three mesoporous samples (NaA-2, 4 and 8) reached almost the same equilibrium capacities within 60 h, despite the difference in adsorption rates. This result indicates that the adsorption capacity is mainly attributed to the microporosity, independent of the degree of mesoporosity. However, in the case of conventional LTA zeolite (NaA-0), the amount of adsorbed xenon even at 60 h was only 15% of the total amount of xenon adsorbed in the hierarchical zeolites.

The diffusion rate can be estimated by using the Fick's second law, which describes the change in the concentration of molecules inside the zeolite crystals as a function of time

$$\frac{\partial C}{\partial t} = D\left(\frac{\partial^2 C}{\partial x^2}\right) \tag{1}$$

In the initial stage of diffusion in zeolite crystals, the following equation is derived from Fick's second law

$$\frac{q(t)}{q(\infty)} = \frac{2}{\sqrt{\pi}}\sqrt{\frac{D}{L^2}}\sqrt{t} \tag{2}$$

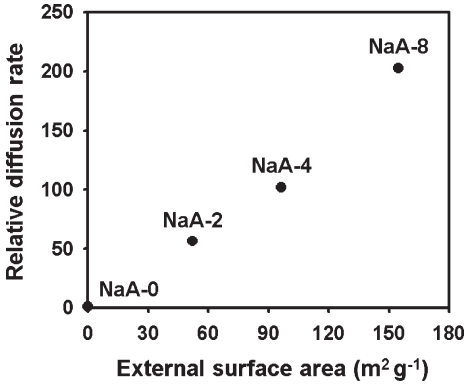

Figure 11. Correlation between diffusion rate and external surface area of LTA zeolite.

where $q(t)/q(\infty)$ is the normalized adsorption quantity, D is the diffusivity of LTA zeolite, L is the characteristic diffusion length, and t is time.[25,42] For the hierarchical zeolites, the normalized adsorption quantity can be derived from dividing xenon uptake by the total adsorbed quantity at equilibrium (t = 60 h). To evaluate a normalized adsorption quantity for NaA-0, we can assume that the adsorbed quantity at equilibrium in NaA-0 would be similar to that in the hierarchical zeolites.

As shown in Figure 10B, the normalized adsorption quantities thus obtained are directly proportional to the square root of t during the initial stage [$q(t)/q(\infty) < 0.6$], according to eq 2. The diffusion rates can then be estimated from the slope of the $t^{1/2}$ versus $q(t)/q(\infty)$ plot. The diffusion rates for NaA-2, NaA-4, and NaA-8, thus obtained are 56, 102, and 203 times higher than that of NaA-0, respectively. The diffusion rates of the hierarchical zeolites are directly proportional to the surface area as shown in Figure 11. Such a tendency of the diffusion property supports our explanation for the rapid xenon diffusion in hierarchical LTA zeolites (Figure 9B).

Effects of Mesoporosity on the Catalytic Conversion of Methanol. To investigate the effect of the facile diffusion in the hierarchical zeolites on catalytic performance, we selected methanol-to-hydrocarbon conversion as a probe reaction. NaA-2 was selected as a mesoporous zeolite for comparison with the conventional NaA-0 zeolite sample. However, a Na^+-exchanged LTA zeolite is not an active catalyst for the conversion of methanol to hydrocarbons compared with the H^+ ion-exchanged MFI zeolite.[43] The acidity of the Na^+-LTA zeolite is not sufficient for methanol conversion. In addition, the diameter of the α-cage aperture (0.42 nm) is not sufficient for diffusion of DME (σ = 0.43 nm). The Ca^{2+} ion exchange in LTA zeolite is known to increase the α-cage aperture to 0.48 nm,[27] which can facilitate the diffusion of DME to a great extent. Because of this, the NaA-0 and NaA-2 samples were used as catalysts after the ion exchange to Ca^{2+}. The unit cell formulas of the resultant zeolites were $Na_{0.2}$-$Ca_{11.8}[(AlO_2)_{12}(SiO_2)_{12}]\cdot 27H_2O$ for CaA-0 and $Na_{0.1}$-$Ca_{11.9}[(AlO_2)_{12}(SiO_2)_{12}]\cdot 27H_2O$ for CaA-2. The Ca^{2+}

(42) Kärger, J.; Ruthven, D. M. *Diffusion in Zeolites and Other Microporous Solids*; Wiley and Sons: New York, 1992.
(43) Stöcker, M. *Microporous Mesoporous Mater*. **1999**, *29*, 3–48.

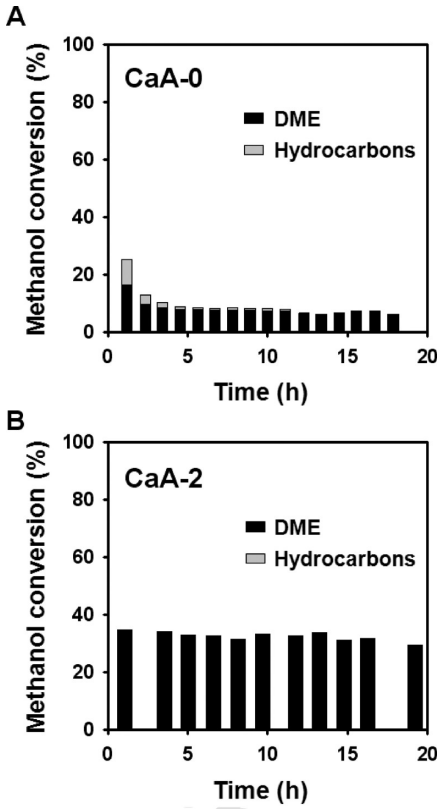

Figure 12. Catalytic conversion of methanol over Ca^{2+} ion-exchanged LTA zeolite (reaction temperature = 673 K, WHSV = 7.5 g g^{-1} h^{-1}): (a) CaA-0 and (b) CaA-2 zeolites. Methanol conversion was calculated by considering dimethyl ether (DME) and hydrocarbons as converted products.

content was analyzed by inductively coupled plasma atomic emission spectroscopy. The CaA-0 catalyst exhibited a much lower conversion rate and higher selectivity to hydrocarbons than those over CaA-2 (Figure 12). The methanol conversion over CaA-0 was 25% during the initial use (at 1 h) under the present reaction condition. The hydrocarbon selectivity was 34%. The major product (66%) was dimethyl ether (DME), which is known as an intermediate species in the methanol conversion.[43] Approximately 2/3 of the hydrocarbon products were light C1−C6 alkanes. However, the hierarchically porous CaA-2 catalyst exhibited the methanol conversion of 34% at 1 h, and the selectivity to hydrocarbons was almost zero. Another notable result is that the conventional zeolite catalyst was deactivated very rapidly compared with the hierarchical zeolite. The catalytic activity of CaA-0 decreased to less than 7% conversion after 5 h, while CaA-2 was deactivated only to 30% even at 21 h. Despite the clear difference in the catalytic performance, the two zeolites exhibited no significant differences in acid strength and acid site density as shown by the temperature-programmed desorption of ammonia in Figure S1 of the Supporting Information.

The mesoporous zeolite exhibited high conversion of methanol, low selectivity to hydrocarbons, and slowed deactivation compared with those of the conventional zeolite counterpart. The difference between CaA-0 and CaA-2 may be explained by facile diffusion of DME because of the micropore−mesopore connectivity as in the case of xenon diffusion. Because the Lenard−Jones σ parameters for DME and Xe are very similar (0.43 for DME versus 0.44 for Xe), it is reasonable to assume similar diffusion properties. The facile diffusion of DME from the zeolite micropores seems to prevent the conversion to hydrocarbons. The catalytic lifetime also seems to increase because of the resultantly low concentration of hydrocarbons before their polymerization to the catalyst-deactivating coke species. Thus, the reaction data suggests that hierarchical LTA zeolite could exhibit significantly different catalytic performance due to improved diffusion property compared with that of solely microporous LTA zeolite. The absence of hydrocarbon products in the case of the mesoporous zeolite can only be explained by the enhanced diffusion. Nonetheless, a possibility of DME production at the external acid sites on the mesopore walls cannot be ignored. The effect of the external acid sites may be further investigated by running the reaction after poisoning the external acidity with bulky pyridine derivatives or may be accounted for by an accessibility index of the external acid sites as suggested by Thibault-Starzyk et al.[44]

Conclusion

In conclusion, synthetic and structural investigations for controlling the mesoporosity in hierarchical LTA zeolite were performed successfully. The structural properties of hierarchical LTA zeolite such as crystal morphology, mesopore diameter, and pore volume were strongly influenced by the amount of surfactant as the mesopore generator. TEM imaging after generating Pt nanowires in mesopores proved that the hierarchical LTA zeolite had a three-dimensional network of mesoporous channels in a fully disordered way. Experimental results showed that the mesopores were not open in the as-synthesized state but could be partially open by solvent extraction of the surfactant. The calcined zeolite exhibited mesopore diameters that were markedly larger than the size of surfactant micelle. On the basis of these results, we propose that the large mesopore diameter of the hierarchical LTA zeolite can arise because of the pore expansion effect by the excessive surfactants. Furthermore, it was possible to expand the mesopore diameters up to 24 nm (beyond the usual 10 nm) by the addition of $EO_{20}PO_{70}EO_{20}$ triblock copolymers as a pore expanding agent. This knowledge on the pore structure and the ability to control the mesopore diameter would be helpful for generation of mesoporosity in other zeolite materials.

In addition, ^{129}Xe NMR demonstrated that the hierarchical LTA zeolites had fully open connectivity between micropores and mesopores. The diffusion rate increased in proportion to the degree of mesoporosity in the hierarchical LTA zeolite. In particular, in the case of

(44) Thibault-Starzyk, F.; Stan, I.; Abelló, S.; Bonilla, A.; Thomas, K.; Fernandez, C.; Gilson, J. -P.; Pérez-Ramírez, J. *J. Catal.* **2009**, *264*, 11–14.

the hierarchical NaA-8 zeolite, the diffusion rate of xenon was approximately 200 times higher compared with that of the conventional NaA zeolite. Because the large surface area of the mesopore walls, xenon atoms can diffuse into the thin nanocrystals very rapidly. Such enhanced diffusion properties can affect catalytic performance, where zeolite is used as a catalyst as demonstrated by the catalytic conversion of methanol. In conclusion, this work has provided a useful insight into the synthesis procedure, mesopore generation mechanism, effects of mesopore generation on molecular diffusion, and catalytic performance of such hierarchically porous zeolites.

Acknowledgment. This work was supported by the National Honor Scientist Program of the Ministry of Education, Science, and Technology in Korea.

Supporting Information Available: NH_3 temperature-programmed desorption profiles for LTA zeolite sample (Figure S1). This material is available free of charge via the Internet at http://pubs.acs.org.